Appl. Phys. B 71, 841–848 (2000) / Digital Object Identifier (DOI) 10.1007/s003400000414

Applied Physics B
Lasers
and Optics

Photorefractive optical properties of volume phase gratings induced in sillenite crystals, when the grating vector lies on the (111) plane

D.G. Papazoglou*, N.C. Deliolanis, A.G. Apostolidis, E.D. Vanidhis

Aristotle University of Thessaloniki, Department of Physics, Solid State Section 313-1, 540 06 Thessaloniki, Greece
(Fax: +30-31/998-019, E-mail: optlab@ccf.auth.gr)

Received: 3 January 2000/Revised version: 6 June 2000/Published online: 13 September 2000 –

Abstract. We study the diffraction efficiency of volume phase gratings in $Bi_{12}GeO_{20}$, when the grating vector, lying on a (111) plane, is at an angle with respect to the crystallographic direction. An external bias field parallel to the direction is applied during recording, thus, the recording conditions depend on the grating vector orientation. The basic parameters determining the diffraction efficiency are the grating vector orientation, the rotatory power and the field-induced linear birefringence (primary and secondary). Analytic expressions for the diffraction efficiency have been obtained by taking into account all the above-mentioned parameters, provided that linearly polarized light is incident on the crystal. In this configuration, the influence of the secondary electro-optic effect (inverse piezoelectric and photoelastic effects) to the diffraction efficiency is actually stronger than the influence of the primary effect. Experimental results are given.

PACS: 42.65.Hw; 42.70.Mp

The electro-optic and optically active photorefractive piezocrystals of the sillenite class ($Bi_{12}GeO_{20}$, $Bi_{12}SiO_{20}$) are currently widely employed as image recording media for optical signal processing and real time holographic interferometry [1–4]. In all device applications a phase grating is recorded in the volume of the crystal [5–7], therefore it is important to study the properties of the induced grating. An important parameter, which strongly affects the diffraction properties, is the grating vector orientation $\boldsymbol{G}$. However, the simultaneous presence of natural optical activity and the electro-optic effect [8–16] complicates the theoretical treatment of light-diffraction phenomena in a photorefractive crystal belonging to the 23 point symmetry group. The complexity of the theoretical treatment is increased by the presence of the secondary electro-optic effect [17, 18] which has to be taken into account since it is comparable, or even greater in some cases [19, 20], to the primary electro-optic effect.

The importance of the secondary electro-optic effect on the photorefractivity of $LiNbO_3$ was first shown by Izvanov et al. [21]. Stepanov et al. [22] used this theory to calculate the photoelastic contribution to the photorefractive effect in cubic crystals. A study of the dependence of the components of the impermeability tensor on an inhomogeneous space charge electric field in cubic crystals was presented by Shandarov et al. [23] followed by Anastassakis [24] and Frey et al. [25]. Analytical solutions for the diffraction efficiency and the two-beam coupling gain of arbitrarily cut cubic gyrotropic crystals were presented by Shepelevich et al. [26] and Sturman et al. [27]. Recently Shepelevich et al. [28] have applied the above-mentioned theory for the optimization of the crystal thickness in order to obtain maximum gain. On the other hand various experimental data for the diffraction efficiency [29, 30] and the two-beam coupling gain [31, 32] in the so-called Huignard configuration revealed that there is strong qualitative and quantitative influence of the secondary electro-optic effect on the diffraction efficiency and the two-beam coupling gain, respectively.

Although the overall theoretical problem is solved now for an arbitrary cut, there is a lack of published experimental data for configurations other than Huignard's. Another interesting configuration is the so-called 111 cut. In this configuration the crystal faces are cut parallel to the (111), $(1\bar{1}0)$, $(\bar{1}\,\bar{1}\,2)$ crystalographic planes, while light propagates parallel to the $[\,\bar{1}\,\bar{1}\,\bar{1}\,]$ crystalographic direction. The 111 cut has only recently been studied, by Shepelevich et al. [33]. In their work Shepelevich et al. presented theoretical analysis and experimental data for the two-beam coupling gain of a 111-cut sillenite crystal, while the grating vector was arbitrarily oriented on a (111) crystalographic plane. One important conclusion of the above-mentioned paper is that in this configuration, contrary to the Huignard configuration, the secondary electro-optic effect "switches on" the polarization dependence of the two-beam coupling gain.

In the present work we calculate the diffraction efficiency of a grating recorded in a 111-cut photorefractive crystal of

*Present address: Foundation for Research and Technology-Hellas (FORTH), Institute of Electronic Structure & Laser, P.O. Box 1527, Vassilika Vouton, Heraklion 711 10, Crete, Greece
(Fax: +30-81/391-305, E-mail: dpapa@iesl.forth.gr)

the sillenite class in the presence of an external bias electric field. The grating vector is arbitrarily oriented on the (111) plane and the external bias electric field is applied along the $[1\,\bar{1}\,0]$ crystallographic direction during recording, thus, the recording conditions do not remain constant as we vary the grating-vector orientation. In order to keep the mathematical analysis simple, the bias electric field is removed during reading of the holographic grating. At first, the periodic perturbations induced in the impermeability tensor by the primary and the secondary electro-optic effects are analytically calculated. Secondly, the space-charge amplitude, a parameter in the previous calculations, is analytically calculated for arbitrary grating-vector orientation. Finally, light propagation and diffraction phenomena are taken into account and the diffraction efficiency is analytically calculated. In order to support our theoretical analysis diffraction efficiency experiments are presented, accompanied with analysis, interpretation and conclusions.

1 Electric-field-induced birefringence

In a photorefractive crystal the space-charge grating is built up along a certain direction. The grating period Λ is much smaller compared to the crystal dimensions, therefore, we treat the photorefractive grating as an infinite one. Under static conditions the space-charge electric field is directed parallel to the grating vector $\boldsymbol{G}$, so we can write $\boldsymbol{E}_{\mathrm{sc}}$ as:

$$\boldsymbol{E}_{\mathrm{sc}} = \boldsymbol{n} E_{\mathrm{sc}}^{\mathrm{o}} \cos(\boldsymbol{G}\cdot\boldsymbol{r})\,, \tag{1}$$

where $E_{\mathrm{sc}}^{\mathrm{o}}$ is the amplitude of the space-charge field and $\boldsymbol{n}$ is the unit vector directed parallel to the grating vector $\boldsymbol{G}$. Since all the crystals exhibiting linear electro-optic effects are also piezoelectric, the piezoelectric coupling will produce local deformation to them [32, 34]. Due to the photoelastic effect, the crystal deformation will in turn locally perturb the components of the impermeability tensor B_{ij}. Consequently, under the effect of the electric field of a holographic grating space-charge electric field, the components of the impermeability tensor of a photorefractive piezoelectric crystal acquire the increments [23]:

$$\begin{aligned} &\Delta B_{mn}^{\mathrm{tot}} = \Delta B_{mn}^{\mathrm{p}} + \Delta B_{mn}^{\mathrm{s}}, \\ &\text{where} \quad \begin{cases} \Delta B_{mn}^{\mathrm{p}} = r_{mnk}^{u} n_k E_{\mathrm{sc}}^{\mathrm{o}} \\ \Delta B_{mn}^{\mathrm{s}} = p_{mnkl}^{E} n_l \gamma_{ki} e_{pij} n_p n_j E_{\mathrm{sc}}^{\mathrm{o}}\,, \end{cases} \end{aligned} \tag{2}$$

where n_i stand for the direction cosines of the unit vector $\boldsymbol{n}$, p corresponds to the contribution of the primary electro-optic effect, s corresponds to the contribution of the secondary electro-optic effect; r_{mnk}^{u}, p_{mnkl}^{E}, e_{pij}, are respectively the components of the electro-optic tensor, the photoelastic tensor and the piezoelectric "stress" tensor of the crystal. γ_{ki} is the inverse of the tensor Γ with components:

$$\Gamma_{ik}^{E} = C_{ijkl}^{E} n_j n_l\,,$$

where C_{ijkl}^{E} are the components of the stiffness tensor (at constant electric field).

Since $Bi_{12}GeO_{20}$ belongs to the 23 symmetry class, only the following independent coefficients exist [17]: one independent electro-optic coefficient $r = r_{231}$, one independent piezoelectric coefficient $e = e_{123}$, four independent photoelastic coefficients $p_1 = p_{1111}$, $p_2 = p_{1122}$, $p_3 = p_{1133}$, $p_4 = p_{2323}$ and three independent elastic coefficients $c_1 = C_{1111}$, $c_2 = C_{1122}$, $c_3 = C_{2323}$. From (2) it is concluded that for all crystals belonging to the 23 symmetry class the main diagonal components B_{ii} of the impermeability tensor are perturbed only by the secondary electro-optic effect since $\Delta B_{ii}^{\mathrm{p}} = 0$ ($r_{iik}^{u} = 0 \Rightarrow \Delta B_{ii}^{\mathrm{p}} = 0$). On the other hand, the non-diagonal components (B_{12}, B_{13}, B_{23}) are affected by a combination of the two effects: the primary electro-optic effect via r (electro-optic coefficient) and the secondary electro-optic effect via e, c_i, p_i (piezoelectric, elastic and photoelastic coefficients).

Let us consider the case of a transmission holographic grating with vector $\boldsymbol{G}$ arbitrarily oriented on the (111) plane, at an angle γ_G with respect to the crystallographic direction $[1\,\bar{1}\,0]$ (Fig. 1). In this case, the direction cosines of the unit vector $\boldsymbol{n}$ on the [100], [010], [001] crystallographic axes can be written as:

$$\begin{aligned} n_1 &= \frac{\sqrt{2}}{2}\cos(\gamma_G) - \frac{\sqrt{6}}{6}\sin(\gamma_G)\,, \\ n_2 &= -\frac{\sqrt{2}}{2}\cos(\gamma_G) - \frac{\sqrt{6}}{6}\sin(\gamma_G)\,, \\ n_3 &= \sqrt{\frac{2}{3}}\sin(\gamma_G)\,. \end{aligned} \tag{3}$$

By applying the general expressions presented in [22] to the 111 cut and after some lengthy but simple calculations, we derive the analytical expressions regarding the induced perturbation of the components of the impermeability tensor from (2) and (3):

$$\begin{aligned} \Delta B_{11} &= -\frac{2e}{3\sqrt{6}} E_{\mathrm{sc}}^{\mathrm{o}} \sin(3\gamma_G) \frac{p_1 A_1 + p_2 A_2 + p_3 A_3}{D}\,, \\ \Delta B_{22} &= -\frac{2e}{3\sqrt{6}} E_{\mathrm{sc}}^{\mathrm{o}} \sin(3\gamma_G) \frac{p_3 A_1 + p_1 A_2 + p_2 A_3}{D}\,, \\ \Delta B_{33} &= -\frac{2e}{3\sqrt{6}} E_{\mathrm{sc}}^{\mathrm{o}} \sin(3\gamma_G) \frac{p_2 A_1 + p_3 A_2 + p_1 A_3}{D}\,, \\ \Delta B_{12} &= \Delta B_{21} = E_{\mathrm{sc}}^{\mathrm{o}} \sqrt{\frac{2}{3}} \sin(\gamma_G) \Big[r + \frac{e p_4}{3D} \\ &\quad \times \Big\{ \Big(2 + \cos(2\gamma_G) + \sqrt{3}\sin(2\gamma_G)\Big) A_1 \\ &\quad + \Big(2 + \cos(2\gamma_G) - \sqrt{3}\sin(2\gamma_G)\Big) A_2 \Big\} \Big]\,, \\ \Delta B_{13} &= \Delta B_{31} = E_{\mathrm{sc}}^{\mathrm{o}} \left(-\frac{\sqrt{2}}{2}\cos(\gamma_G) - \frac{\sqrt{6}}{6}\sin(\gamma_G) \right) \\ &\quad \times \Big[r + \frac{e p_4}{3D} \Big\{ 4\sin^2(\gamma_G) A_1 \\ &\quad + \Big(2 + \cos(2\gamma_G) - \sqrt{3}\sin(2\gamma_G)\Big) A_3 \Big\} \Big]\,, \\ \Delta B_{23} &= \Delta B_{32} = E_{\mathrm{sc}}^{\mathrm{o}} \left(\frac{\sqrt{2}}{2}\cos(\gamma_G) - \frac{\sqrt{6}}{6}\sin(\gamma_G) \right) \\ &\quad \times \Big[r + \frac{e p_4}{3D} \Big\{ 4\sin^2(\gamma_G) A_2 \\ &\quad + \Big(2 + \cos(2\gamma_G) + \sqrt{3}\sin(2\gamma_G)\Big) A_3 \Big\} \Big]\,, \end{aligned} \tag{4}$$

where the parameters A_1, A_2, A_3, D are given by the equations:

$$
\begin{aligned}
A_1 = &-(c_1-c_2-2c_3)\,(c_1+2c_2+c_3)\\
&\times\left(\frac{2}{9}\cos^4(\gamma_G)+\frac{2}{3\sqrt{3}}\cos^3(\gamma_G)\sin(\gamma_G)\right)\\
&+\frac{1}{9}\left[c_1^2-2c_2^2+c_1\,(c_2-4c_3)-11c_2c_3-5c_3^2\right]\cos^2(\gamma_G)\\
&+\frac{\sqrt{3}}{9}\left[2c_1^2+2c_1c_2+c_1c_3-(2c_2+c_3)^2\right]\cos(\gamma_G)\sin(\gamma_G)\\
&+\frac{1}{36}\,(4c_1-c_2-5c_3)\,(c_1-c_2-2c_3)\\
&-\frac{1}{6}c_3\,(c_1+2c_2+c_3)+c_1c_3\,,\\
A_2 = &-(c_1-c_2-2c_3)\,(c_1+2c_2+c_3)\\
&\times\left(\frac{2}{9}\cos^4(\gamma_G)-\frac{2}{3\sqrt{3}}\cos^3(\gamma_G)\sin(\gamma_G)\right)\\
&+\frac{1}{9}\left[c_1^2-2c_2^2+c_1\,(c_2-4c_3)-11c_2c_3-5c_3^2\right]\cos^2(\gamma_G)\\
&-\frac{\sqrt{3}}{9}\left[2c_1^2+2c_1c_2+c_1c_3-(2c_2+c_3)^2\right]\cos(\gamma_G)\sin(\gamma_G)\\
&+\frac{1}{36}\,(4c_1-c_2-5c_3)\,(c_1-c_2-2c_3)\\
&-\frac{1}{6}c_3\,(c_1+2c_2+c_3)+c_1c_3\,,\\
A_3 = &\frac{4}{9}\,(c_1-c_2-2c_3)\,(c_1+2c_2+c_3)\cos^4(\gamma_G)\\
&-\frac{2}{9}\left[c_1^2-2c_2^2+c_1\,(c_2-4c_3)-11c_2c_3-5c_3^2\right]\cos^2(\gamma_G)\\
&+\frac{1}{36}\,(c_1-7c_2-8c_3)\,(c_1-c_2-2c_3)\\
&-\frac{2}{3}c_3\,(c_1+2c_2+c_3)+c_1c_3\,,\\
D = &-\frac{1}{108}\Big\{(c_1-c_2-2c_3)^2\,(c_1+2c_2+c_3)\cos(6\gamma_G)\\
&-c_1^3-24c_3c_1^2-2\,(c_2+2c_3)\left(c_2^2+c_3^2-11c_2c_3\right)\\
&+3c_1\left(c_2^2+2c_3c_2-18c_3^2\right)\Big\}\,. \qquad (5)
\end{aligned}
$$

The birefrigent characteristics of the perturbed crystal can be studied with the help of the optical indicatrix. For cubic $Bi_{12}GeO_{20}$ the indicatrix is a sphere which, in the presence of an electric field, is transformed into an ellipsoid. Referring to the elliptic cross section of the indicatrix with the (111) plane we can easily prove that the refraction index variation amplitude of the crystal, along the principal axes (Ox', Oz') of the ellipse (Fig. 1), is given by the equations:

$$
\begin{aligned}
\Delta n^{\mathrm{o}}_{x'} = &-\frac{1}{12}n_{\mathrm{o}}^3\Big\{2\Big(\Delta B_{11}+\Delta B_{22}+\Delta B_{33}-\Delta B_{12}\\
&-\Delta B_{13}-\Delta B_{23}\Big)+\Big[(\Delta B_{11}+\Delta B_{22}-2\Delta B_{33}\\
&-4\Delta B_{12}+2\Delta B_{13}+2\Delta B_{23})^2\\
&+3(\Delta B_{22}-\Delta B_{11}+2\Delta B_{13}-2\Delta B_{23})^2\Big]^{\frac{1}{2}}\Big\}\,,
\end{aligned}
$$

$$
\begin{aligned}
\Delta n^{\mathrm{o}}_{z'} = &-\frac{1}{12}n_{\mathrm{o}}^3\Big\{2\Big(\Delta B_{11}+\Delta B_{22}+\Delta B_{33}-\Delta B_{12}\\
&-\Delta B_{13}-\Delta B_{23}\Big)-\Big[(\Delta B_{11}+\Delta B_{22}-2\Delta B_{33}\\
&-4\Delta B_{12}+2\Delta B_{13}+2\Delta B_{23})^2\\
&+3(\Delta B_{22}-\Delta B_{11}+2\Delta B_{13}-2\Delta B_{23})^2\Big]^{\frac{1}{2}}\Big\}\,, \qquad (6)
\end{aligned}
$$

where n_{o} is the refraction index of the unperturbed crystal. The angle ψ between the principal axis Ox' and the $[1\,\bar{1}\,0]$ direction is calculated as:

$$
\tan(2\psi) = \frac{\sqrt{3}\,(\Delta B_{22}-\Delta B_{11}+2\Delta B_{13}-2\Delta B_{23})}{\Delta B_{11}+\Delta B_{22}-2\Delta B_{33}-4\Delta B_{12}+2\Delta B_{13}+2\Delta B_{23}}\,. \qquad (7)
$$

2 Calculation of the space-charge field amplitude

For long grating periods (over 10 μm) a holographic grating is recorded in a $Bi_{12}GeO_{20}$ crystal by applying an external electric field to it (drift regime) [35, 36]. In this case, the recording conditions are not constant for an arbitrary grating vector orientation γ_G. Consequently, the induced space-charge concentration and the space-charge field amplitude depend on the grating vector orientation γ_G [37].

In this study high voltage is applied to the $(1\,\bar{1}\,0)$ faces of the crystal (Fig. 1). To calculate the space-charge field dependence on the angle γ_G we assume that, during recording, the externally applied electric field produces a spatial displacement $\boldsymbol{d}_{\mathrm{o}}$ to the photoexited electron distribution. Also, $\boldsymbol{d}_{\mathrm{o}}$ is always parallel to the direction of the bias field and remains fairly constant for any grating vector orientation.

The sum of the positive and the negative space-charge distributions equals the total space charge distribution. Therefore, the amplitude $\varrho^{\mathrm{o}}_{\mathrm{sc}}$ of the total space-charge distribution

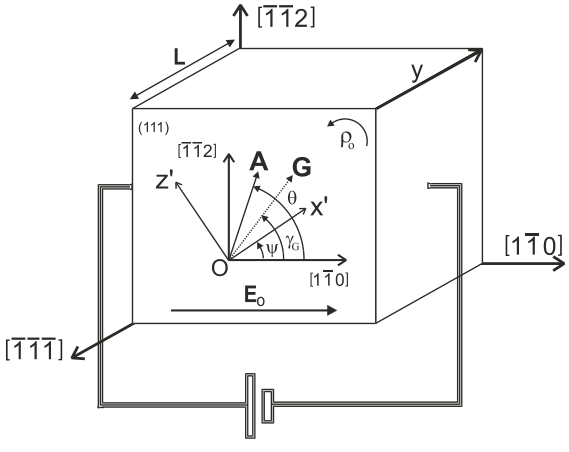

Fig. 1. Crystallographic orientation of the BGO crystal. The bias electric field is parallel to the $[1\,\bar{1}\,0]$ direction, Ox' and Oz' are the axes of linear birefringence induced by the space-charge field with grating vector $\boldsymbol{G}$, oriented at an angle γ_G to the $[1\,\bar{1}\,0]$ direction. The general direction of light propagation is normal to the (111) plane. The angle θ represents the polarization orientation of the readout beam **A** and is measured anticlockwise to the $[1\,\bar{1}\,0]$ direction

is [30, 37, 38]:

$$\varrho_{sc}^{o} \propto \cos(\gamma_G)\,, \quad \frac{d_o}{\Lambda} \ll 1\,, \tag{8}$$

thus, for sufficiently small displacements, the space-charge amplitude is proportional to $\cos(\gamma_G)$.

On the other hand [32, 34], the effective static dielectric constant relating the space-charge amplitude ϱ_{sc}^{o} and the space-charge field amplitude E_{sc}^{o} is perturbed by the piezoelectric effect. Thus, in order to calculate the functional relationship between ϱ_{sc}^{o} and E_{sc}^{o}, the compressional and shear deformation that arise from piezoelectricity should be taken into account. In the case of a holographic grating, with grating vector arbitrarily oriented on the (111) section, we obtain the following equation by combining the crystal deformation [30] with the expression for the dielectric response of a piezoelectric crystal [17] and the Poisson equation:

$$\begin{aligned}\varrho_{sc}^{o} = G E_{sc}^{o}\Big\{\epsilon\epsilon_o + \frac{e^2}{9D}\big[8\sqrt{3}(A_1 - A_2)\cos(\gamma_G)\sin^3(\gamma_G) \\ - (A_1 + A_2 - 2A_3)\left(\cos(4\gamma_G) + 2\cos(2\gamma_G)\right) \\ + 3(A_1 + A_2 + A_3)\big]\Big\}\,,\end{aligned} \tag{9}$$

where ϵ_o, ϵ are respectively the vacuum primitivity and the relative dielectric constant (for constant strain), and A_1, A_2, A_3, D parameters already defined in (5).

Consequently, using (8) and (9), the amplitude of the space-charge field can be calculated as:

$$\begin{aligned}E_{sc}^{o} = \alpha E_o \cos(\gamma_G)\Big\{1 + \frac{e^2}{9D\epsilon\epsilon_o}\Big[8\sqrt{3}\,(A_1 - A_2)\cos(\gamma_G) \\ \times \sin^3(\gamma_G) - (A_1 + A_2 - 2A_3)\big(\cos(4\gamma_G) + 2\cos(2\gamma_G)\big) \\ + 3(A_1 + A_2 + A_3)\Big]\Big\}^{-1}\,,\end{aligned} \tag{10}$$

where E_o is the bias electric field amplitude and α is simply a scaling parameter calculated by fitting the theoretical curves to the experimental data (see forward, Fig. 7 and (12)). The parameter α actually integrates the effect of the modulation, the grating period and other "recording" parameters and is invariant to the grating vector orientation. In Fig. 2 we plot the space-charge field amplitude E_{sc}^{o} versus γ_G calculated from (10) with and without taking into account the secondary electro-optic effect. The crystal parameters $r = 3.14\,\mathrm{pm/V}$ [9], $\varrho_o = 20.5°/\mathrm{mm}$, $e = 0.98\,\mathrm{C/m^2}$, $p_1 = 0.12$, $p_2 + p_3 = 0.19$, $p_4 = 0.01$, $c_1 = 12.84 \times 10^{10}\,\mathrm{N/m^2}$, $c_2 = 2.94 \times 10^{10}\,\mathrm{N/m^2}$, $c_3 = 2.55 \times 10^{10}\,\mathrm{N/m^2}$ [22, 39, 40] and $\epsilon = 51.5$ are used in the calculations. The external field used was $E_o = 6\,\mathrm{kV/cm}$ and the calculated value of the scaling parameter was $\alpha = 0.548$. The two curves practically coincide except for the range of $-30° < \gamma_G < 30°$. In this case, the secondary electro-optic effect flattens the cosine peak of the curve, therefore, a fairly constant space-charge field is induced in the crystal for this range of grating vector orientation.

In Fig. 3, we plot the induced perturbations ΔB_{ij} in the components of the impermeability tensor B_{ij} calculated from (4). As it can be observed, the main diagonal components of the impermeability tensor are perturbed only by the secondary electro-optic effect and they are almost equal

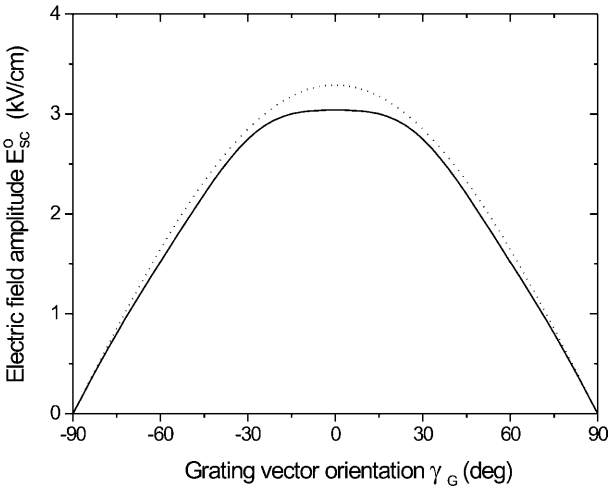

Fig. 2. Theoretically calculated space-charge field amplitude as a function of the grating vector orientation γ_G. $(\cdots)$ = the theoretical curve calculated without taking into account the secondary electro-optic effect ($e = 0\,\mathrm{C/m^2}$), (—) = the theoretical curve calculated with the secondary electro-optic effect taken into account ($e = 0.98\,\mathrm{C/m^2}$)

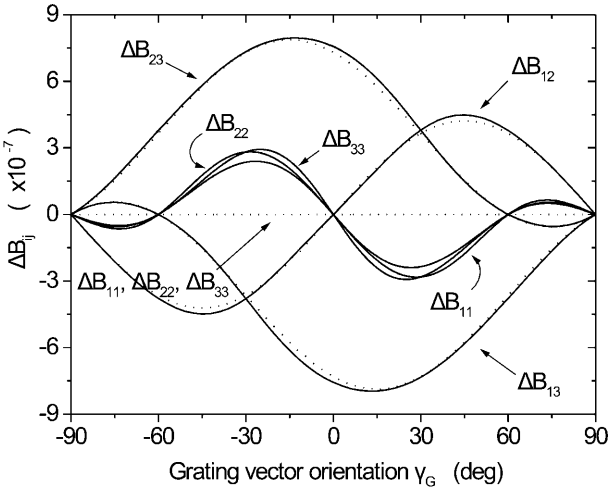

Fig. 3. Theoretically calculated perturbations ΔB_{ij} of the components of the impermeability tensor as a function of the grating vector orientation γ_G. $(\cdots)$ = theoretical curves calculated without taking into account the secondary electro-optic effect ($e = 0\,\mathrm{C/m^2}$), (—) = theoretical curves calculated with the secondary electro-optic effect taken into account ($e = 0.98\,\mathrm{C/m^2}$)

to each other ($\Delta B_{11} \approx \Delta B_{22} \approx \Delta B_{33}$). This is due to the fact that for $Bi_{12}GeO_{20}$ $p_1 \approx p_2 \approx p_3$ and therefore the sums $(p_1A_1 + p_2A_2 + p_3A_3)$, $(p_3A_1 + p_1A_2 + p_2A_3)$, $(p_2A_1 + p_3A_2 + p_1A_3)$ in the numerators of (4) are almost equal to each other. On the other hand, the secondary electro-optic effect has a minor contribution in the perturbation of the non-diagonal components of the impermeability tensor (ΔB_{12}, ΔB_{13}, ΔB_{23}) and it could be easily neglected. Concluding, the perturbation of the components of the impermeability tensor is qualitatively different for the two effects, since the secondary electro-optic effect perturbs the main diagonal components of the impermeability tensor, while the primary electro-optic effect perturbs only the non-diagonal components of B_{ij}.

In Fig. 4, we plot the amplitude of the periodic variations $\Delta n^{o}_{x'}$, $\Delta n^{o}_{z'}$ of the refractive index of the crystal versus γ_G defined in (6), with and without taking into account the secondary electro-optic effect. As it is clearly seen, the presence of the secondary electro-optic effect disturbs the symmetry $|\Delta n^{o}_{x'}| = |\Delta n^{o}_{z'}|$ obtained for $e = 0\,\mathrm{C/m^2}$ (taking into account only the primary electro-optic effect).

In Fig. 5, we plot the orientation ψ of the principal axis Ox' with respect to the $[1\,\bar{1}\,0]$ crystallographic direction versus the angle γ_G calculated from (7), with and without taking into account the secondary electro-optic effect. Contrary to the previous plots, the orientation ψ is practically not affected by the secondary electro-optic effect. This is due to the fact that in (7) the perturbations ΔB_{ii} of the diagonal components of the impermeability tensor cancel each other (they are almost equal). Therefore, the orientation ψ depends on the non-diagonal components (ΔB_{12}, ΔB_{13} and ΔB_{23}) of the impermeability tensor, which in turn are perturbed mainly by the primary electro-optic effect.

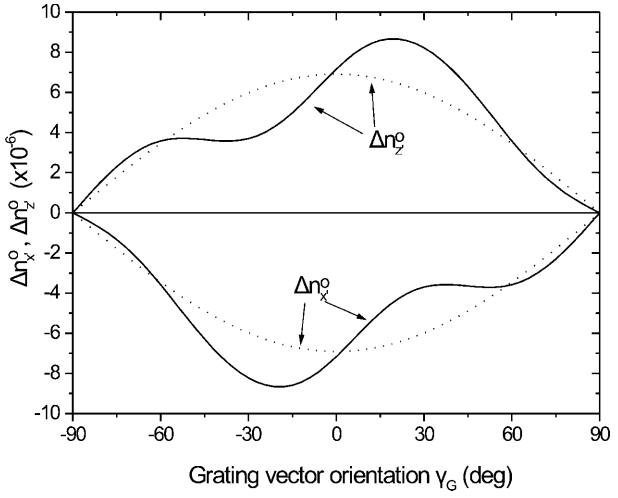

Fig. 4. Theoretically calculated perturbations $\Delta n^{o}_{x'}$, $\Delta n^{o}_{z'}$ of the refractive index as a function of the grating vector orientation γ_G. $(\cdots)$ = theoretical curves calculated without taking into account the secondary electro-optic effect ($e = 0\,\mathrm{C/m^2}$), (—) = theoretical curves calculated with the secondary electro-optic effect taken into account ($e = 0.98\,\mathrm{C/m^2}$)

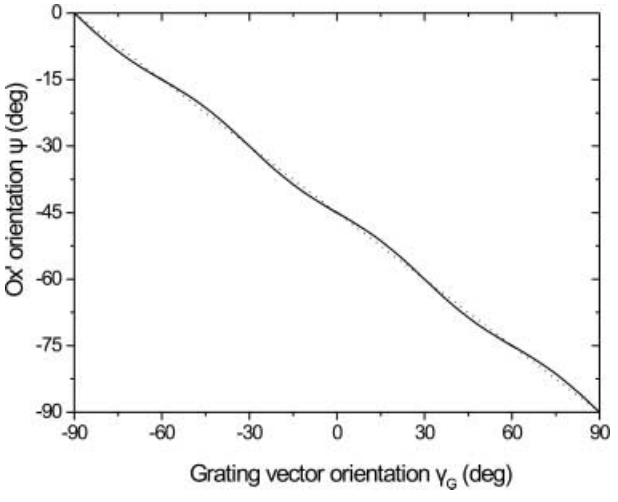

Fig. 5. Theoretically calculated orientation ψ of the principal Ox' axis as a function of the grating vector orientation γ_G. $(\cdots)$ = theoretical curves calculated without taking into account the secondary electro-optic effect ($e = 0\,\mathrm{C/m^2}$), (—) = theoretical curves calculated with the secondary electro-optic effect taken into account ($e = 0.98\,\mathrm{C/m^2}$)

3 Outline of the procedure followed for the analytical calculation of the diffraction efficiency

Assuming a non-depleted readout beam, the electric field amplitude of the diffracted beam is obtained by the vector summation of diffracted electric field amplitudes, which result from successive cross sections along the crystal depth. The crystal geometry presented in Fig. 1 is used to describe for the following analysis. The angle between the grating vector and the $[1\,\bar{1}\,0]$ crystallographic direction is γ_G and the probe beam is incident at the Bragg angle. Since the spatial frequency of the grating is low, both the probe and the diffracted beams are assumed to propagate in the y ([111]) direction. In order to keep the mathematical analysis simple we consider that no bias field is applied to the crystal during the reading process. Since the induced grating is weak, the propagation of light in the crystal can be studied assuming that the crystal presents optical activity without linear birefringence. Also, the linear birefringence is taken into account in order to calculate the diffracted amplitude, but is neglected for studying the propagation of the direct and the diffracted beams [9]. When plane polarized monochromatic light is transmitted through an isotropic crystal presenting optical activity, the plane of polarization is rotated by an angle ϱ_o per unit length.

A linearly polarized beam $\boldsymbol{A}$ (Fig. 1) vibrating at an angle θ with respect to the direction $[1\,\bar{1}\,0]$ is used to read the grating. The incident light polarization plane will rotate through an angle $\varrho_o l$ in the anti-clockwise direction on traversing a thickness l of the crystal. The readout beam is diffracted by a thin elementary grating of thickness dl situated at a depth l from the entrance face of the crystal. The elementary diffracted amplitude components, along the Ox' and Oz' principal axes, rotate further through an angle $\varrho_o(L-l)$ (where L is the crystal thickness) while propagating through the remaining crystal thickness. By integrating all the elementary diffracted amplitude components emerging from the crystal over the crystal thickness, we obtain the total diffracted amplitude and, hence, the diffraction efficiency [30, 37]:

$$\eta = R + Q\cos(2\theta + \phi)\,, \tag{11}$$

where:

$$\begin{aligned} R &= \frac{\pi^2 L^2}{4\lambda^2}\left[(\Delta n^{o}_{x'} + \Delta n^{o}_{z'})^2 + (\Delta n^{o}_{x'} - \Delta n^{o}_{z'})^2 \mathrm{sinc}^2(\varrho_o L)\right], \\ Q &= \frac{\pi^2 L^2}{2\lambda^2}\left[(\Delta n^{o}_{x'})^2 - (\Delta n^{o}_{z'})^2\right]\mathrm{sinc}(\varrho_o L)\,, \\ \phi &= \varrho_o L - 2\psi\,. \end{aligned} \tag{12}$$

Thus, for an arbitrary grating vector orientation, the diffraction efficiency η is a cosine function of the readout beam polarization angle θ with amplitude Q, dc level R and phase ϕ. The input polarization angle $\theta_{\max}$ required to obtain maximum diffraction efficiency $\eta = R + |Q|$ is directly

related to the phase ϕ and the sign of the amplitude Q by the equation:

$$\theta_{\max} = \begin{cases} -\frac{\phi}{2} = \psi - \frac{1}{2}\varrho_{\mathrm{o}} L\,, & Q > 0\,, \\ -\frac{\phi}{2} + 90^{\circ} = \psi - \frac{1}{2}\varrho_{\mathrm{o}} L + 90^{\circ}\,, & Q < 0\,, \end{cases} \tag{13}$$

as it can be readily obtained from (11).

4 Experiment

In this section we present the experimental procedure and discuss the anisotropic optical properties of volume phase gratings that are induced in a BGO crystal and are arbitrarily oriented on a (111) plane. A schematic diagram of the experimental set-up is given in Fig. 6. A collimated beam of quasi-monochromatic light obtained from a Xe-Hg high-pressure white lamp illuminates a Ronchi grating. The lenses L_1 and L_2 form an image of the grating in the BGO crystal. The apertures a_1, a_2 in the diaphragm D transmit the ± 1 diffracted orders of the grating. A second diaphragm D′ with a single aperture a′ lies in the image plane of D, and a photomultiplier (PM) is placed after D′. By changing the interference filter (IF) we can use different wavelengths, the Bragg condition being automatically satisfied for all wavelengths without any modification of the experimental arrangement. A variable grating vector orientation is achieved by rotating the Ronchi grating.

During the recording process we use green light (546 nm), polarizer P is removed, and high voltage (6 kV/cm) is applied to the crystal. On the other hand, during the reading process we use red light (645 nm), polarizer P is put back in place, no high voltage is applied to the crystal and aperture a_1 is closed. In our experiments we use an undoped $10 \times 9 \times 5$ mm BGO crystal. The crystal is illuminated over its entire surface.

In Fig. 7 the amplitude $|Q|$ and the dc level R of the diffraction efficiency η versus the grating vector orientation γ_G are shown. Besides the experimental points referring to the amplitude $|Q|$ and the dc level R, two sets of theoretically calculated curves, using (12), are drawn. In the first set the contribution of the inverse piezoelectric ($e = 0.98\,\mathrm{C/m^2}$) and, consequently, the secondary electro-optic effects are taken into account. On the other hand, in the second set, the secondary electro-optic effect is not taken into account ($e = 0\,\mathrm{C/m^2}$). Clearly, there is a discrete difference both in magnitude and in shape between the respective curves of the two sets. The most interesting is that the amplitude $|Q|$ of the diffraction efficiency η is equal to zero if we do not take the secondary electro-optic effect into account

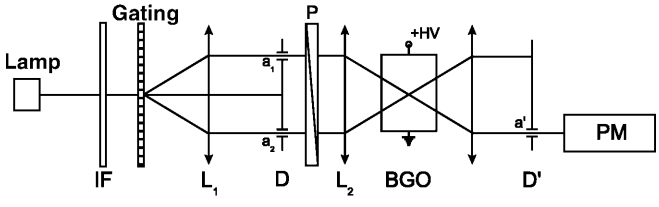

Fig. 6. The experimental set-up. (IF): interference filter, (L_1, L_2): lenses, (D, D′): diaphragms, (P): graduated linear polarizer step motor controlled, (+HV): high voltage, (PM): photomultiplier

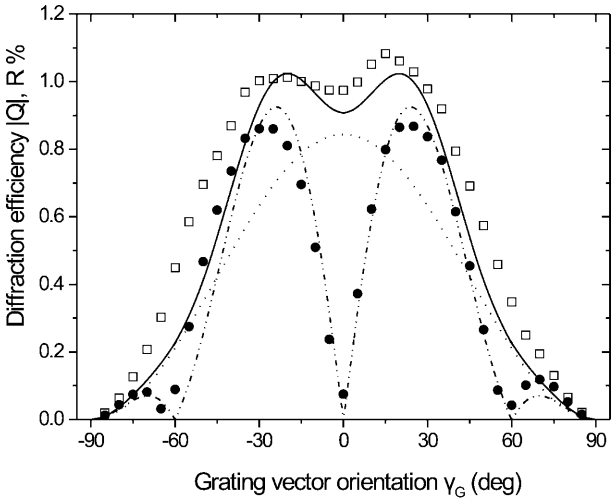

Fig. 7. Comparison of the experimentally measured diffraction efficiency amplitude $|Q|$ and dc level R with the theoretically calculated ones as a function of the grating vector orientation γ_G. □ = the experimental points for R, (—) = the theoretical curve for R calculated with the secondary electro-optic effect taken into account ($e = 0.98\,\mathrm{C/m^2}$), (· · ·) = the theoretical curve for R calculated without taking into account the secondary electro-optic effect ($e = 0\,\mathrm{C/m^2}$), ● = the experimental points for $|Q|$, — · · — = the theoretical curve for $|Q|$ calculated with the secondary electro-optic effect taken into account ($e = 0.98\,\mathrm{C/m^2}$), $|Q| = 0$ if we do not take the secondary electro-optic effect into account in our calculations

($e = 0\,\mathrm{C/m^2} \Rightarrow |Q| = 0$). The dc level R of the diffraction efficiency η is not greatly affected by the presence of the secondary electro-optic effect, and reaches maximum for grating vectors oriented at about $\pm 20^{\circ}$ to the crystallographic direction. The fit between the theoretical results and the experimental data is very satisfactory when we take inverse piezoelectric and, consequently, the secondary electro-optic effect into account.

In Fig. 8 the maximum diffraction efficiency $\eta_{\max}$ versus the grating vector orientation γ_G is shown. Both theoretical and experimental results show that the optimum conditions

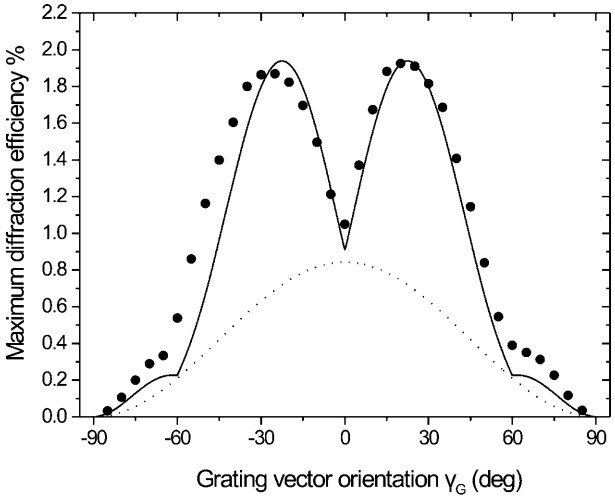

Fig. 8. Comparison of the experimentally measured maximum diffraction efficiency with the theoretically calculated one as a function of the grating vector orientation γ_G. ● = the experimental points, (—) = the theoretical curve calculated with the secondary electro-optic effect taken into account ($e = 0.98\,\mathrm{C/m^2}$), · · · = the theoretical curve calculated without taking into account the secondary electro-optic effect ($e = 0\,\mathrm{C/m^2}$)

for the hologram readout are achieved when the holographic grating is oriented at about $\pm 20^\circ$ with respect to the crystallographic direction. In this case, the maximum diffraction efficiency $\eta_{\max}$ increases about twice compared with its value at $\gamma_G = 0^\circ$.

Finally, in Fig. 9 the input polarization angle $\theta_{\max}$, required to obtain maximum diffraction efficiency, versus the angle γ_G is shown. Equations (7) and (13) are used for the calculations. The fit between the theoretical results and the experimental data is excellent when we take the secondary electro-optic effect into account ($e = 0.98\,\mathrm{C/m^2}$) and very poor when the secondary electro-optic effect is not taken into account ($e = 0\,\mathrm{C/m^2}$). From the theoretical point of view, $\theta_{\max}$ is determined by the orientation ψ of the Ox' refractive axis and the sign of the diffraction efficiency amplitude Q. Although the angle ψ remains practically unaffected by the presence of the secondary electro-optic effect (see Fig. 5), the amplitude Q is greatly affected by the presence of the secondary electro-optic effect, since $Q = 0$ for $e = 0\,\mathrm{C/m^2}$ (see Fig. 7).

5 Conclusions

We have analyzed the anisotropic optical properties of volume phase holographic gratings induced in a BGO photorefractive crystal. The grating vector is considered to be arbitrarily oriented on the (111) crystallographic plane and a bias field is applied parallel to the $[1\bar{1}0]$ direction during grating recording. The primary, along with the secondary, electro-optic effects are taken into account. A non-depleted readout beam is assumed and energy transfer effects are neglected. Explicit analytic expressions are deduced for the space-charge field amplitude $E_{\mathrm{sc}}^{\mathrm{o}}$, the induced perturbations ΔB_{ij} in the components of the impermeability tensor, the respective perturbations $\Delta n_{x'}^{\mathrm{o}}$, $\Delta n_{z'}^{\mathrm{o}}$ of the refractive index, the orientation ψ of the principal Ox' axis and, finally, for the diffraction efficiency η. Although the theoretical analysis is quite complex, it is still possible to deduce simple and elegant analytic expressions. The diffraction efficiency is a simple sinusoidal function of the reading vector polarization orientation.

The physical parameters that determine the diffraction efficiency are the polarization orientation of the readout beam, the crystal thickness, the rotatory power and the field-induced birefringence (primary and secondary). The diffraction efficiency is strongly affected by the presence of the secondary electro-optic effect. If we neglect the role of the secondary electro-optic effect, we are led to the false result that the diffraction efficiency is independent of the polarization orientation of the readout beam (Q=0). Our results agree favorably with the results of Shepelevich et al. [33].

On the other hand, the functional dependence of the diffraction efficiency versus the grating vector orientation is a complex function of the configuration [29, 30, 33]. Specifically, the diffraction efficiency amplitude Q and the dc level R are intricate functions of the grating vector orientation γ_G. The functional dependence of Q and R to γ_G is determined by the configuration (i.e. the crystal geometry) and the crystal parameters (i.e. the rotatory power etc.). An alteration of the configuration results in a respective qualitative and quantitative modification of the functional dependence of R and Q. Therefore, it is possible to obtain a desired functional dependence of the diffraction efficiency versus the grating vector orientation by properly choosing the configuration.

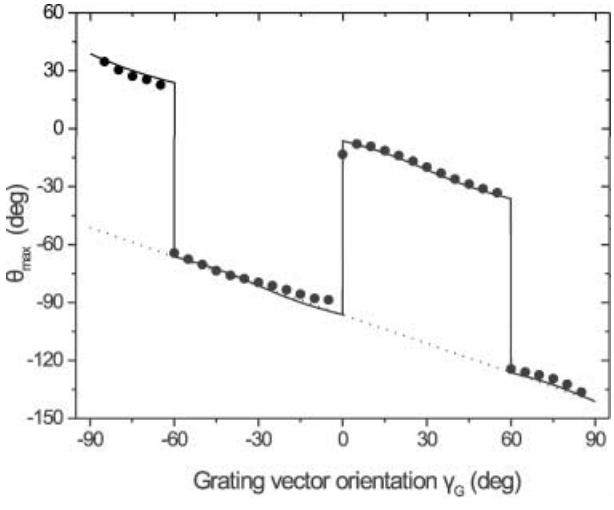

Fig. 9. Comparison of the experimentally measured input polarization angle $\theta_{\max}$, required to obtain maximum diffraction efficiency with the theoretically calculated one as a function of the grating vector orientation γ_G. ● = the experimental points, (—) = the theoretical curve calculated with the secondary electro-optic effect taken into account ($e = 0.98\,\mathrm{C/m^2}$), $\cdots$ = the theoretical curve calculated without taking into account the secondary electro-optic effect ($e = 0\,\mathrm{C/m^2}$)

Acknowledgements. One of the authors (N.C. Deliolanis) is kindly supported by the Greek State Scholarship Foundation.

References

1. J.P. Huigniard, F. Micheron: Appl. Phys. Lett. **29**, 591 (1976)
2. M. Tebaldi, L.A. Toro, M.D. Lasprilla, N. Bolognini: Opt. Commun. **155**, 342 (1998)
3. J.P. Herriau, J.P. Huignard, A.G. Apostolidis, S. Mallick: Opt. Commun. **56**, 141 (1985)
4. L. Labrunie, G. Pauliat, J. C. Launay, S. Leidenbach, G. Roosen: Opt. Commun. **140**, 119 (1997)
5. D. Tontchev, S. Zhivkova, M. Miteva: Appl. Opt. **29**, 4753 (1990)
6. G. Roosen, M. T. Plantegenest: Ferroelectrics **56**, 137 (1984)
7. A.A. Kamshilin, J. Frejlich, L. Cescato: Appl. Opt. **25**, 2375 (1986)
8. S. Mallick, D. Rouede, A.G. Apostolidis: J. Opt. Soc. Am. B **4**, 1247 (1987)
9. A.G. Apostolidis, S. Mallick, D. Rouede, J.P. Herriau, J.P. Huignard: Opt. Commun. **56**, 73 (1985)
10. G. Pauliat, G. Roosen: Ferroelectrics **75**, 281 (1987)
11. J.R. Goff: J. Opt. Soc. Am. B **12**, 99 (1995)
12. H.C. Pedersen, P.M. Johansen: J. Opt. Soc. Am. B **12**, 592 (1995)
13. P. Yeh: J. Opt. Soc. Am. B **4**, 1382 (1987)
14. D.J. Webb, A. Kießling, B.I. Sturman, E. Shamonina, K.H. Ringhofer: Opt. Commun. **108**, 31 (1994)
15. A. Brignon, K.H. Wagner: Opt. Commun. **101**, 239 (1993)
16. E. Shamonina, V.P. Kamenov, K.H. Ringhofer, G. Cedilnik, A. Kießling, R. Kowarschik, D.J. Webb: Opt. Commun. **146**, 62 (1998)
17. J.F. Nye: *Physical Properties of Crystals* (Oxford University Press, Oxford 1957)
18. Y.I. Sirotin, M.P. Shaskolskaya: *Fundamentals of Crystal Physics* (Mir, Moskow 1982)
19. H.C. Ellin, L. Solymar: Opt. Commun. **130**, 85 (1996)
20. G. Montemezzani, A.A. Zozulya, L. Czaia, D. Z. Anderson, M. Zgonik, P. Gunter: Phys. Rev. A **52**, 1791 (1995)
21. A.A. Izvanov, A.E. Mandel, N.D. Khatkov, S.M. Shandarov: Sov. Autometria **2**, 79 (1986)

22. S.I. Stepanov, S.M. Shandarov, N.D. Khatkov: Sov. Phys. Solid State **29**, 1754 (1987)
23. S.M. Shandarov, V.V. Shepelevich, N.D. Khatkov: Opt. Spectrosc. **70**, 627 (1991)
24. E. Anastassakis: IEEE J. Quantum Electron. **QE-29**, 2239 (1993)
25. L. Frey, G. Pauliat, J. Jonathan, M. Dumont, G. Roosen: Appl. Phys. B **68**, 999 (1999)
26. V.V. Shepelevich: Opt. Spectrosc. **83**, 161 (1997)
27. B.I. Sturman, E.V. Podivilov, K.H. Ringhofer, E. Shamonina, V.P. Kamenov, E. Nippolainen, V. Prokofief, A.A. Kamshilin: Phys. Rev. E **60**, 3332 (1999)
28. V.V. Shepelevich, Y. Hu, A. Firsov, E. Shamonina, K.H. Ringhofer: Appl. Phys. B **68**, 923 (1999)
29. V.V. Shepelevich, S.M. Shandarov, A.E. Mandel: Ferroelectrics **110**, 235 (1990)
30. D.G. Papazoglou, A.G. Apostolidis, E.D. Vanidhis: Ferroelectrics **205**, 87 (1998)
31. V.V. Shepelevich, N.N. Egorov, V. Shepelevich: J. Opt. Soc. Am. B **11**, 1394 (1994)
32. G. Pauliat, P. Mathey, G. Roosen: J. Opt. Soc. Am. B **8**, 1942(1991)
33. V.V. Shepelevich, S.F. Nichiporko, A.E. Zagorskiy, N.N. Egorov, Y. Hu, K.H. Ringhofer, E. Shamonina: In *Advances in Photorefractive Materials, Effects, and Devices*, Vol. 27 of OSA TOPS (1999) p. 353
34. P. Günter, M. Zgonik: Opt. Lett. **16**, 1826 (1991)
35. J.J. Amodei: RCA Rev. **32**, 185 (1971)
36. N.V. Kukhtarev, V.B. Markov, S.G. Odoulov, M.S. Soskin, V.L. Vinetskii: Ferroelectrics **22**, 949 (1979)
37. D.G. Papazoglou: Ph.D. Thesis, (Aristotle University of Thessaloniki, Thessaloniki 1997)
38. A.G. Apostolidis, E.D. Vanidhis, D.G. Papazoglou: Synthetic Metals **83**, 287 (1996)
39. M.P. Shaskolskaya: *Acoustic Crystals* (Nauka, Moskow 1982)
40. V.V. Kucha, V.I. Mirgorodskii, S.V. Peshin, A.T. Sobolev: Sov. Tech. Phys. Lett. **10**, 51 (1984)